25 February 2000

ELSEVIER

Chemical Physics Letters 318 (2000) 393–401

CHEMICAL PHYSICS LETTERS

www.elsevier.nl/locate/cplett

Symmetry and lifetime of the hydroxymethyl radical in the 3p Rydberg state

V. Aristov, D. Conroy, H. Reisler *

Department of Chemistry, University of Southern California, Los Angeles, CA 90089-0482, USA

Received 8 September 1999; in final form 25 November 1999

Abstract

Hydroxymethyl (CH_2OH) radicals were produced in a molecular beam via the photoinitiated reaction between Cl atoms and methanol. The rovibronic spectrum obtained following excitation to the 3p Rydberg state was measured by $(1+1)$ and $(2+1)$ REMPI. Analyses of rotational contours of selected vibronic bands obtained in the molecular beam and in a flow cell led to the assignment of the excited Rydberg state as $^2A''(3p_z)$. The 11 ± 2 cm^{-1} homogeneous linewidth that best fits the observed contours implies a lifetime of the excited state of 0.5 ± 0.1 ps, consistent with predissociative decay.

1. Introduction

The hydroxymethyl radical (CH_2OH) has attracted considerable research interest due to practical and scientific considerations. It is involved in pyrolytic and oxidative pathways of methanol combustion, and may also participate in reactions that affect the atmosphere. The C–H bond in methanol is weaker than the O–H bond, favoring pyrolytic formation of CH_2OH, and because CH_2OH is also more reactive than its isomer, the methoxy radical (CH_3O), understanding its dissociative and reactive pathways is important. It is not surprising, therefore, that a large body of research has been devoted to this radical [1]. Nevertheless, little is currently known about the electronic spectroscopy of CH_2OH [1–5], its photophysics, and photochemistry [6–10], due mainly to difficulties in preparing it in clean, well-defined environments. CH_2OH is an attractive candidate for collision-free studies of photoinitiated reactions, since several allowed dissociative pathways are open on the different electronic potential energy surfaces (PESs), and isomerization to the methoxy radical may precede decomposition. In addition, the small size of the radical should facilitate comparisons with high-level electronic structure and dynamical calculations.

In this Letter, we describe the first spectroscopic study of CH_2OH in a molecular beam. Specifically, we report the rotational contours of selected vibronic bands in the electronic transition between the ground state and an excited 3p Rydberg state. From the spectroscopic analysis we deduce the symmetry of the electronic transition, characterize the 3p state, and conclude that it must be predissociative. We also describe in some detail our method of producing cold beams (~ 10 K) of the radical.

* Corresponding author. Fax: +1-213-746-4945; e-mail: reisler@chem1.usc.edu

0009-2614/00/$ - see front matter
PII: S0009-2614(00)00042-7

Our studies rely on the careful spectroscopic work of Hudgens and co-workers who recorded and assigned the vibronic structure of the same transition using (2 + 1) and (1 + 1) resonance-enhanced multiphoton ionization (REMPI) detection [1,4]. Dulcey and Hudgens [4], and Bomse et al. [3] observed an intense (2 + 1) REMPI spectrum in the region 430–490 nm, which they ascribed to a two-photon transition from the singly occupied π^*_{CO} molecular orbital in the electronic ground state to a 3p Rydberg state, $3p \leftarrow \pi^*$. Johnson and Hudgens [1] extended this study to the 'hot band' region of the radical using both (2 + 1) and (1 + 1) REMPI. They also carried out ab initio electronic structure calculations of the ground electronic state of the neutral molecule and its cation, concentrating on the out-of-plane vibrational motions in the OH torsion and CH_2 wag modes. It was concluded that as a result of the shallowness of the CH_2 wag angular potential, CH_2OH behaves spectroscopically in accordance with C_s symmetry selection rules, despite the nonplanarity of the molecule at its potential minima. This conclusion led to reassignment of some of the vibronic bands.

Rettrup et al. calculated ab initio vertical excitation energies to several Rydberg states [11]. They found that the lowest excited states can be classified (in ascending order) as the 3s, $3p_x$, $3p_y$ and $3p_z$ Rydberg-type orbitals. Based on correspondence with spectral structures in the measured 300 K absorption spectrum of CH_2OH [5], and the calculated order and energies of the transitions, they proposed that the Rydberg state accessed in the REMPI studies is the $3p_x$ state, which is of A′ symmetry.

In our studies, hydroxymethyl radicals are produced in a molecular beam by using the photoinitiated reaction of methanol with chlorine atoms. Table 1 lists the most important chemical processes involved in the reactive production of CH_2OH. At room temperature (and below), Cl atoms are energetically incapable of removing the hydroxyl hydrogen and producing the methoxy radical [15]; however, 355 nm photolysis of Cl_2 produces Cl atoms with ~ 50 kJ mol^{-1} of translational energy. In our experiments, Cl atom translation is quenched prior to reaction by multiple collisions with buffer gas atoms. The $CH_2OH + Cl$ reaction is ten times faster than the production reaction, underlining the need to adjust conditions to disfavor consumption of the radical. These conditions have been found by carrying out kinetic modeling using the rate constants given in Table 1 [18].

2. Experimental

The greatest challenge in these experiments has been the development of a stable pulsed-beam source of expansion-cooled hydroxymethyl radicals. Formation of a greenish liquid has been observed on metal surfaces exposed to methanol/chlorine gas mixtures, and hydroxymethyl radical production is not observed when the reactant mixture passes over this liquid. Therefore, the gas handling system has been carefully designed to allow only non-metallic, corrosion-resistant materials to contact the reactant mixture (Pyrex, Teflon, Ultem 3040, and Kalrez 4079). Additionally, the expanding mixture passes briefly over quartz and a small amount of sodium silicate adhesive. Even under these conditions, stable operation requires frequent cleaning of the gas delivery line and the nozzle.

Reactant mixtures of Cl_2, CH_3OH and He are prepared in a glass and Teflon gas-delivery line.

Table 1
Reactive processes in the production of CH_2OH

Reaction	ΔH^o(298 K) (kJ mol^{-1})	Rate constant (cm^3 molecule^{-1} s^{-1})
$Cl_2 \rightarrow^{355\ nm} 2Cl$	-94.28 ± 0.01 [12]	
$Cl + CH_3OH \rightarrow HCl + CH_2OH$	-29.3 ± 2.0 [1,12–14]	$(6.1 \pm 0.6) \times 10^{-11}$ [15]
$Cl + CH_3OH \rightarrow HCl + CH_3O$	8.4 ± 1.8 [12,14,16]	
$Cl + CH_2OH \rightarrow HCl + CH_2O$	-115.9 ± 6.6 [1,12,13]	$(6.6 \pm 1.3) \times 10^{-10}$ [5]
$2CH_2OH \rightarrow$ products		1.5×10^{-11} [17]

First, methanol is allowed to evaporate ($\sim$ 100 Torr) into a 5.0 l glass reservoir. Next, a 5% Cl_2/He mixture is added in an amount adjusted to achieve a final 1–2% Cl_2 concentration. Last, helium is added to a total pressure of 3 atm.

Reactant mixtures are introduced into the vacuum chamber through a modified piezoelectrically-driven pulsed nozzle ($\sim$ 250 μs FWHM) shown in Fig. 1 [19]. The faceplate of a conventional nozzle has been replaced with an o-ring gland, through which runs an extended plunger. To this gland is fitted a small chamber into which the reactant mixture is delivered, and which is terminated by a faceplate with a 0.6 mm orifice. Approximately the same pressure of buffer gas is maintained inside the main chamber of the piezoelectric nozzle to prevent leakage across the o-ring gland seal and to facilitate normal plunger movement. The plunger, gland, reactant chamber, and faceplate were manufactured from glass-fiber-reinforced polyetherimide (Ultem 3040), and the o-rings on the plunger are made of Kalrez 4079.

The reactant mixture flows into the vacuum chamber through a $\sim$ 10 mm long quartz tube ($\sim$ 1 mm i.d.) affixed to the faceplate with sodium silicate adhesive. This arrangement is similar to that utilized by Lester and co-workers [20]. Photodissociation of Cl_2 is achieved with the tripled output of a Nd:YAG laser (Quanta-Ray DCR-1, 355 nm, 8 mJ) directed onto the quartz tube. In order to avoid overly sensitive dependence upon the photolysis laser focus position and timing, a 30 cm focal length (f.l.) cylindrical lens is employed, with the lens axis aligned parallel to the quartz tube and its focal point located slightly beyond the tube. In this way, a section of $\sim$ 2 mm along the expanding reactant mixture is uniformly illuminated in the convergent portion of the photolysis beam. The relative rates of the production and consumption reactions of the radicals (Table 1) mandate that the photoinitiation region be located near the end of the quartz tube in order to minimize subsequent collisions of CH_2OH with Cl atoms.

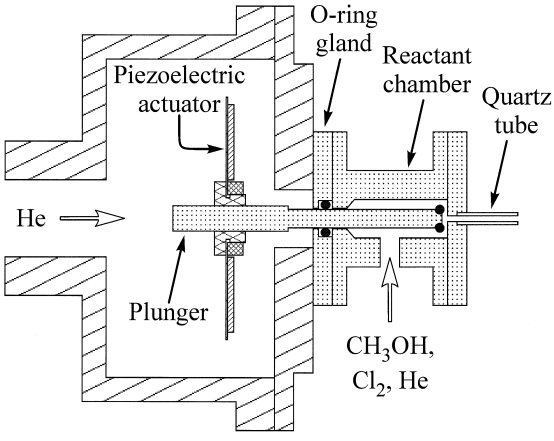

Fig. 1. Schematic cross-section of the modified pulsed nozzle. The mechanical support for the piezoelectric actuator has been omitted for clarity.

Chlorine reactant (Airgas West, 99.5%) is purified by freezing in an ethyl acetate slush (189 K) followed by pumping for several minutes to remove HCl. It is then combined in a corrosive-resistant gas cylinder with helium (Airgas West, 99.999%) to yield a 5% Cl_2/He mixture by volume. Methanol (Mallinckrodt absolute, low acetone) is degassed and stored in a glass bulb under vacuum.

The vacuum apparatus consists of two differentially pumped chambers: a source chamber pumped through a liquid-nitrogen cold trap by a diffusion pump, and a detection chamber evacuated by a turbomolecular pump. The source and detection chambers are joined by a flange on which a skimmer is mounted. The effluent of the nozzle is skimmed (Beam Dynamics, 1.51 mm) at a distance of $\sim$ 10 mm from the quartz tube and passes into the detection region. The pressure in the detection region is $\sim 2 \times 10^{-7}$ Torr with the nozzle operating at 10 Hz, while the base pressure is $\sim 1 \times 10^{-7}$ Torr.

Cl, HCl, and CH_2OH are detected with a combination of REMPI spectroscopy and time-of-flight (TOF) mass spectrometry. REMPI is achieved using the focussed, linearly polarized output of an excimer-pumped dye laser system (Lambda-Physik EMG201/LPD3000 or COMPEX/FL3002, Coumarin 440, 450, 460, 480). In the 1-color (2 + 1) REMPI scheme, tunable 440–490 nm radiation (2 mJ, 50 cm f.l. lens) is focused at the center of the detection chamber. In the 2-color (1 + 1) REMPI detection scheme, absorption of a focused, 220–245 nm photon (0.2 mJ, 100 cm f.l. lens) excites the radical resonantly to the 3p Rydberg state, while a second, 440–490 nm, photon (2 mJ) ionizes the excited molecule. In the 2-color scheme, the fundamental and frequency doubled laser beams co-propa-

gate into the chamber, and the intensities are adjusted to ensure that the 3p state is accessed predominantly via one-photon absorption.

Ions are accelerated (2.5 keV) towards a multichannel plate (MCP) detector (Galileo, 25 mm) through a Wiley–McLaren 19 cm TOF mass spectrometer [21], which is mounted vertically. The MCP output is amplified, digitized and transferred to a computer that averages the signals and records portions of the TOF trace. A dedicated software package has been developed for this purpose, allowing the simultaneous recording of ion signals of up to five masses as a function of the REMPI laser wavelength or delay time. Time delays are controlled with delay generators, and the dye laser grating steps are controlled by the computer. Laser wavelengths are calibrated using known frequencies of Cl and HCl REMPI lines [22,23].

Under typical operating conditions, the Cl atom pulse duration is ~ 250 μs FWHM at the detection region, while the corresponding CH_2OH pulse width is shorter, ~ 100 μs, and concentrated at the leading edge of the Cl atom pulse. The efficiency of CH_2OH production depends sensitively on the position of the Cl_2 photolysis pulse, and the pressures and ratios of Cl_2 and methanol. The molecular beam temperature is estimated at ~ 6 K from the rotational temperature of a beam of 2% NO in He, while the corresponding temperature of the CH_2OH radical is ~ 10 K (see Section 3).

3. Results and discussion

3.1. REMPI spectra of CH_2OH

Unsaturated 1-color (2 + 1) and 2-color (1 + 1) REMPI spectra of expansion-cooled CH_2OH radicals excited via the 3p Rydberg state are shown in Fig. 2. The spectra are similar to those previously

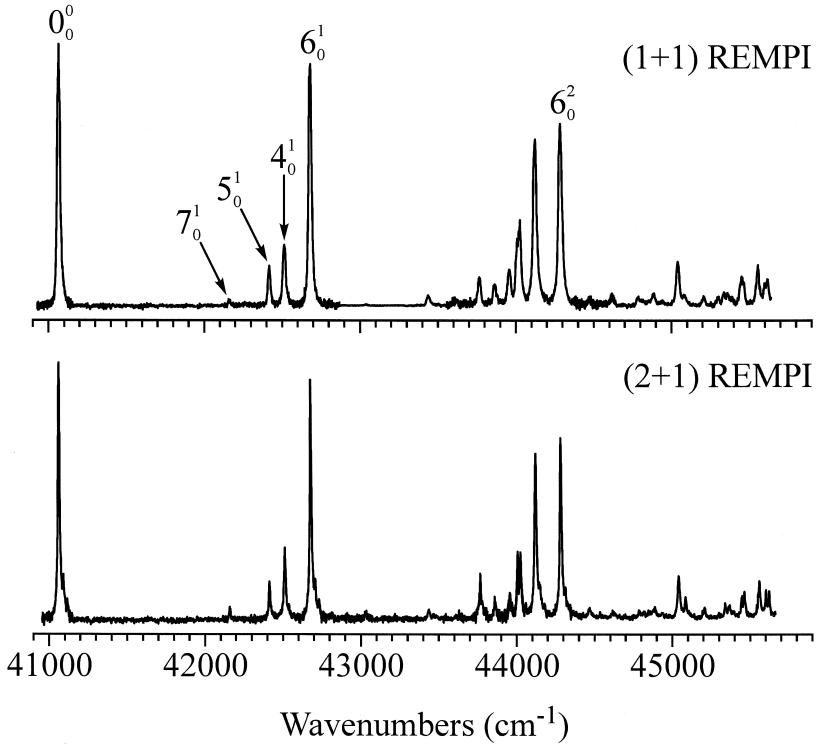

Fig. 2. Unsaturated (2 + 1) and (1 + 1) REMPI spectra of CH_2OH obtained in a molecular beam, showing vibronic structure. Each spectrum is a composite of several data sets, smoothed 5–10 points and normalized to the laser power. Some vibronic assignments are indicated [1,3,4]. The bottom scale shows $3p \leftarrow \pi^*$ excitation energy.

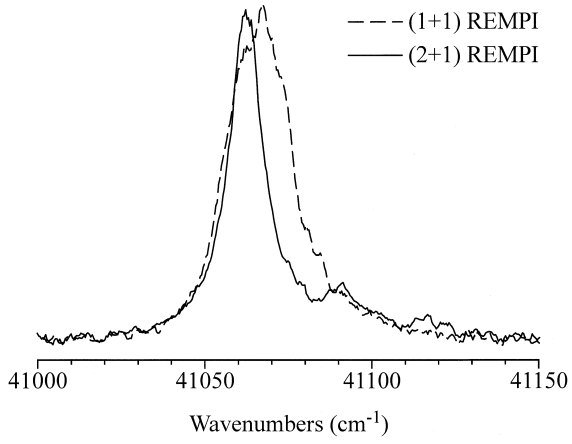

Fig. 3. Expanded view of the origin band obtained by (1 + 1) and (2 + 1) REMPI. Notice the narrower width of the main feature in the (2 + 1) REMPI spectrum.

observed in 300 K samples [1,3,4]. Non-saturated conditions are verified by observing the spectral intensities and bandwidths as a function of excitation laser energies. Dulcey and Hudgens reported the vibrational assignment of the (2 + 1) spectrum based on a normal mode analysis [4]. Bands at ~41 640 and ~42 010 cm^{-1} were assigned to the 8_0^1 and 9_0^1 vibronic transitions, which have mixed CH_2 wag and OH torsion character [4]. Based on more recent (1 + 1) and (2 + 1) spectra (especially from vibrationally excited CH_2OH) and ab initio calculations, Johnson and Hudgens concluded that CH_2OH complied spectroscopically with the C_s point group. This caused reassignment of these bands as the 9_1^1 and 8_1^1 vibronic 'hot bands', respectively [1]. Consistent with the new assignments, these features are weakly observed in our expansion-cooled spectra only under saturated conditions.

Although the vibrational features in the (2 + 1) and (1 + 1) spectra appear nearly identical, distinct differences in band shapes are apparent upon closer inspection. As can be seen in Fig. 3, which displays the (1 + 1) and (2 + 1) origin bands peaking at 41 067 and 41 062 cm^{-1}, respectively, the most intense feature in the (1 + 1) REMPI spectrum is wider than that in the (2 + 1) spectrum. The latter spectrum has two small features on the blue side of the band maximum. These shapes are common to all isolated vibronic bands, and as a consequence, some vibronic bands appear resolved in the (2 + 1) spectrum but not in the (1 + 1) spectrum. Despite rotational cooling in the molecular beam and the 0.3 cm^{-1} laser bandwidth, no individual rotational lines are resolved in either spectrum.

3.2. Simulations of the (2 + 1) and (1 + 1) REMPI spectra

Both the one- and two-photon rotational contours of the origin band are compared with computer simulations. The rotational constants are derived from the geometries of the ground and excited states obtained ab initio [1], and are given in Table 2. The asymmetry parameters for the ground and excited states are −0.95 and −0.94, respectively, justifying the use of prolate-top rotor energies and selection rules. The rotational constant is taken as the average value of the calculated asymmetric rotor rotational constants B and C. To generate simulated spectra, each rotational line is broadened by a Lorentzian lineshape (see below), and the superposition of the Lorentzians within a vibronic band is calculated at 0.08 cm^{-1} intervals.

The shape of the simulated rotational contour of each vibronic band in the one-photon transition to the 3p state is determined by the orientation of the transition dipole moment relative to the symmetry axis, the relevant selection rules and Hönl–London linestrengths, the rotational state population distribution, and the line broadening function. For one-photon parallel transitions ($\Delta N = 0, \pm 1$; $\Delta K = 0$), the spectrum consists of three ΔN branches ($^{Q}P, {}^{Q}Q, {}^{Q}R$, where the superscript indicates the ΔK branch). For perpendicular transitions ($\Delta N = 0, \pm 1$; $\Delta K = \pm 1$), each of the P, Q, and R branches has R and P sub-branches and the spectrum consists of six branches ($^{P}P, {}^{R}P, {}^{P}Q, {}^{R}Q, {}^{P}R, {}^{R}R$). The selection rules for the two-photon transitions ($\Delta N = 0, \pm 2$; $\Delta K = 0, \pm 2$) [24] give rise to nine branches

Table 2
Rotational constants of the ground and 3p states of CH_2OH

Rotational constant	A (cm^{-1})	B (cm^{-1})	C (cm^{-1})
Ground state	6.624	1.014	0.876
3p state	6.697	1.156	0.996

(^{O}O, ^{Q}O, ^{S}O, ^{O}Q, ^{Q}Q, ^{S}Q, ^{O}S, ^{Q}S, ^{S}S). The linestrengths for one-photon electronic transitions of symmetric top rotors are taken from Herzberg [24], and those for two-photon transitions (with parallel polarizations of the two photons) have been derived by Chen and Yeung [25]. A Boltzmann rotational population distribution is assumed, with the degeneracies given by $2(2N+1)$ for $K>0$, and $(2N+1)$ for $K=0$, and the rotational temperature and homogeneous width of the rotational lines are varied to achieve the best fit with the experimental results.

Typical simulations of rotational contours of vibronic bands are compared with the corresponding observations in Fig. 4. Simulations with parallel and perpendicular orientations of the transition dipole moment relative to the C_s symmetry axis (i.e., the CO bond axis [1]) are shown in the first and second columns, respectively. Both columns show also the

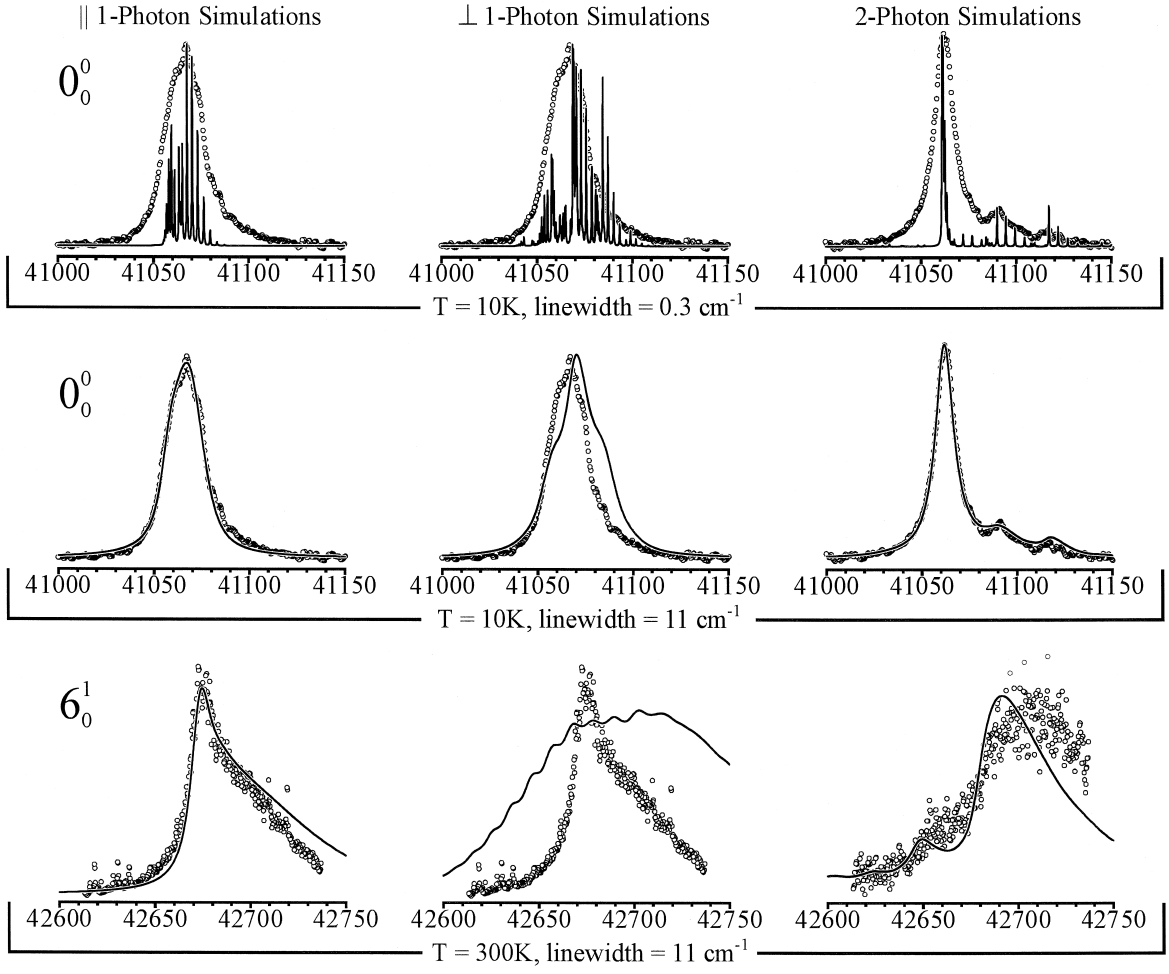

Fig. 4. The solid lines display simulations of rovibronic bands of the $3p \leftarrow \pi^*$ transition assuming either one-photon parallel or perpendicular transitions, or a two-photon transition with parallel polarizations of the photons. The circles show the corresponding measured vibronic bands obtained via (1 + 1) and (2 + 1) REMPI (first two columns and third column, respectively). In the upper two rows, the 0_0^0 vibronic bands obtained in a molecular beam are shown, while the bottom row displays the 6_0^1 spectra obtained in a flow cell. The bottom scales show the excitation energies to the 3p state with the vibronic band origin estimated at 41 060 cm^{-1}, and the energies of the 6_0^1 bands adjusted to match the observed maxima.

observed 2-color $(1+1)$ REMPI spectra. The third column presents the experimental $(2+1)$ REMPI spectra and simulations of the two-photon $3p \leftarrow \pi^*$ transition. The first row shows simulated rotational spectra of the vibronic origin band assuming a 10 K Boltzmann rotational distribution and 0.3 cm^{-1} linewidth. In the second row, 10 K simulations of the same band are presented, but with 11 cm^{-1} linewidth; these are the parameters that best fit the observed spectra. The third row displays 300 K simulations of the 6_0^1 band using 11 cm^{-1} linewidth, together with the corresponding experimental REMPI spectra obtained in a separate flow cell following the reaction of Cl atoms with methanol [18].

The lower panel of Fig. 5 illustrates how the different rotational branches contribute to the overall vibronic band shapes in the two-photon $3p \leftarrow \pi^*$ transition. At 10 K, there are four dominant branches: ^{Q}Q $(\Delta N=0,\ \Delta K=0)$, ^{S}S $(\Delta N=+2,\ \Delta K=+2)$, ^{Q}S $(\Delta N=+2,\ \Delta K=0)$, and ^{S}Q $(\Delta N=0,\ \Delta K=+2)$. These branches originate from the lowest rotational levels, which have large populations at 10 K. The rotational lines of the strongest band, ^{Q}Q, lie very close to the electronic transition origin, resulting in the tall, narrow feature observed in the two-photon spectrum. The second strongest band is the ^{S}S band, which gives rise to the two features located

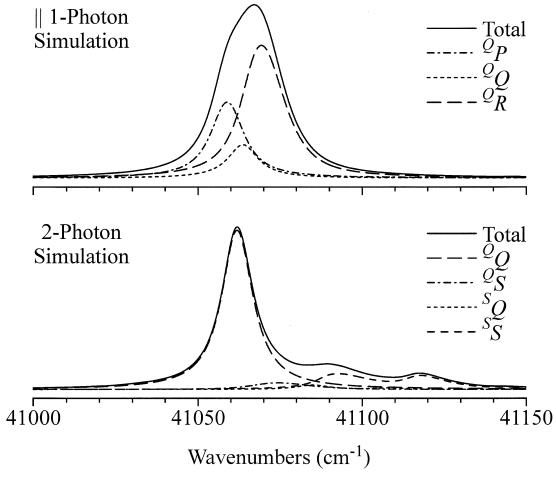

Fig. 5. Detail of the dominant branches obtained from simulations of a parallel one-photon (upper panel) and a two-photon transition with parallel polarizations of the photon (bottom panel). Prolate rotor spectral lines are convoluted with a Lorentzian broadening function of 11 cm^{-1} FWHM.

to the blue of the ^{Q}Q band and spans a wide energy range. Although the ^{S}Q and ^{Q}S bands contribute noticeably to the overall intensity, they are spread in energy and do not give rise to prominent features.

In contrast to the two-photon transition, the ^{Q}Q band for the corresponding one-photon parallel transition, depicted in the upper panel of Fig. 5, is the weakest, and the ^{Q}R and ^{Q}P bands are spread more widely around the electronic origin. Blended together, the three bands yield a contour of twice the width of the ^{Q}Q band in the two-photon spectrum. Because of the $\Delta K \pm 1$ selection rule, the contours obtained for the $(1+1)$ perpendicular transition are even broader (Fig. 4).

We note that because of the double-well structure in the torsional and CH_2 wag vibrational modes, the hydroxymethyl radical belongs to the G_4 permutation–inversion group (isomorphic with the C_{2v} point group) rather than the C_s point group. The G_4 group should be used whenever the parity splittings are substantial and/or the rotational levels are high. Under such conditions, the couplings between the angular momenta of the torsion/internal rotor and molecular rotation should be considered explicitly, as well as effects due to nuclear spin statistics. However, the results of Johnson and Hudgens show that in the low levels of the ground and 3p states (i.e., at the bottom of the torsional well), the splittings of the parity levels are < 0.1 cm^{-1} [1], while the lifetime broadening determined by us is 11 cm^{-1}. Therefore, the two parity states are excited simultaneously. Under these conditions, and considering the low rotational excitation of 10 K CH_2OH, use of the C_s point group in the simulations of the rotational contours reported here is justified.

3.3. Comparisons with measured spectra and the symmetry of the electronic transition

From the simulations shown in the first row of Fig. 4, it is clear that our ~ 0.3 cm^{-1} laser bandwidth is sufficient to resolve CH_2OH rotational lines in the absence of other broadening factors. The existence of a clear vibronic structure indicates that the 3p Rydberg state is bound; yet the best fit, which is obtained with a simulated linewidth of 11 ± 2 cm^{-1}, corresponds to a 3p state lifetime of 0.5 ± 0.1

ps, which is characteristic of predissociation. This conclusion provides the justification for using Lorentzian lineshapes in the simulations.

The band shapes of the 2-color $(1+1)$ REMPI spectrum measured in the molecular beam are fit well only when assuming a parallel transition. As shown in Fig. 4, the flow-cell data confirm this conclusion, since the 300 K band contours for parallel and perpendicular transitions are very different. Therefore, we conclude that the one-photon transition dipole moment must be aligned parallel to the symmetry axis, i.e. the transition dipole moment must be of A′ symmetry.

It has been shown that CH_2OH possesses C_s point group symmetry in its vibronic transitions to the 3p Rydberg states, and therefore its ground state can be labeled $1\,^2A''$ [1]. Since the electronic transition moment is of A′ symmetry, the excited state must have A″ symmetry. The only 3p Rydberg state of A″ symmetry is $3p_z$, where the z axis is perpendicular to the plane of symmetry of the molecule. Therefore, we assign the excited state as the $3p_z$ Rydberg state, labeling it $2\,^2A''(3p_z)$. This assignment differs from the previous tentative assignment of this transition [5,11] as $1\,^2A'(3p_x) \leftarrow 1\,^2A''$. The previous assignment was based on ab initio calculations of the energies of the Rydberg states [11], and the correspondence with features in the low-resolution 300 K absorption spectrum [5]. Note that the calculations place the vertical excitation energy to the $3p_z$ state at 5.65 eV [11], reasonably close to the observed band origin at 5.10 eV, and also predict a large oscillator strength for the $3p_z \leftarrow \pi^*$ transition.

4. Conclusions

CH_2OH radicals were produced in a molecular beam via the photoinitiated reaction between Cl atoms and methanol. The rotational contours of $(1+1)$ and $(2+1)$ CH_2OH REMPI vibronic bands were measured in the molecular beam and in a flow cell. Comparisons of these spectra with simulations of a homogeneously broadened prolate symmetric top led to reassignment of the excited Rydberg state from $^2A'(3p_x)$ to $^2A''(3p_z)$. The 11 cm^{-1} homogeneous linewidth that best fits the observed contours implies a lifetime of the excited state of 0.5 ± 0.1 ps, consistent with predissociative decay.

Acknowledgements

We wish to thank J. Hudgens and I. Slagle for helpful discussions regarding the production and spectroscopy of the hydroxymethyl radical, A. Suits for the design of the pulsed nozzle, and Lin Feng for careful review of the manuscript. Support by the US Department of Energy, Office of Basic Energy Sciences, Division of Chemical Sciences, is gratefully acknowledged.

References

[1] R.D. Johnson, J.W. Hudgens, J. Phys. Chem. 100 (1996) 19874, and references therein.
[2] J.M. Dyke, A.R. Ellis, N. Jonathan, N. Keddar, A. Morris, Chem. Phys. Lett. 111 (1984) 207.
[3] D.S. Bomse, S. Dougal, R.L. Woodin, J. Phys. Chem. 90 (1986) 2640.
[4] C.S. Dulcey, J.W. Hudgens, J. Chem. Phys. 84 (1986) 5262.
[5] P. Pagsberg, J. Munk, A. Sillesen, C. Anastasi, Chem. Phys. Lett. 146 (1988) 375.
[6] G.F. Adams, R.J. Bartlett, G.D. Purvis, Chem. Phys. Lett. 87 (1982) 311.
[7] D. Solgadi, J.P. Flament, Chem. Phys. 98 (1985) 387.
[8] S.P. Walch, J. Chem. Phys. 98 (1993) 3076.
[9] S.-C. Kuo, Z. Zhang, R.B. Klemm, J.F. Liebman, L.J. Stief, F.L. Nesbitt, J. Phys. Chem. 98 (1994) 4026.
[10] Q. Cui, K. Morokuma, Chem. Phys. Lett. 263 (1996) 54.
[11] S. Rettrup, P. Pagsberg, C. Anastasi, Chem. Phys. 122 (1988) 45.
[12] M.W. Chase, C.A. Davies, J.R. Downey, D.J. Frurip, R.A. McDonald, A.N. Syverud, J. Phys. Chem. Ref. Data 14 (1985) .
[13] S. Dóbé, T. Bérces, T. T, F. Márta, J. Grussdorf, F. Temps, H.G. Wagner, J. Phys. Chem. 100 (1996) 19864.
[14] J.B. Pedley, R.D. Naylor, S.P. Kirby, Thermochemical Data of Organic Compounds, Chapman and Hall, New York, 1986.
[15] S. Dóbé, M. Otting, F. Temps, H.G. Wagner, H. Ziemer, Ber. Bunsenges. Phys. Chem. 97 (1993) 877.
[16] D.L. Osborn, D.J. Leahy, E.M. Ross, D.M. Neumark, Chem. Phys. Lett. 235 (1995) 484.
[17] U. Meier, H.H. Grotheer, G. Riekert, Th. Just, Ber. Bunsenges. Phys. Chem. 89 (1985) 325.
[18] D. Conroy, V. Aristov, unpublished data.
[19] A. Suits, private communication.

[20] M.T. Berry, M.R. Brustein, M.I. Lester, Chem. Phys. Lett. 153 (1988) 17.
[21] W.C. Wiley, I.H. McLaren, Rev. Sci. Instrum. 26 (1955) 1150.
[22] C.E. Moore, Atomic Energy Levels as Derived from the Analyses of Optical Spectra, Natl. Bur. Stand., Washington, DC, 1971.
[23] R. Callaghan, S. Arepelli, R.J. Gordon, J. Chem. Phys. 86 (1987) 5273.
[24] G. Herzberg, Molecular Spectra and Molecular Structure III. Electronic Spectra and Electronic Structure of Polyatomic Molecules, Van Nostrand Reinhold, New York, 1966.
[25] K.M. Chen, E.S. Yeung, J. Chem. Phys. 69 (1978) 43.